Journal of Engineering in Industrial Research

2026, Volume 7, Issue 2

Original Research Article

Improved Physical Properties of Zirconium Incorporation into the Iattice of Chromium Telluride Material

Ernest Ogheneruona Ojegu[1], Akpata Erhieyovwe[1], Clever Kate Ojoba[2], Mike Onyekachukwu Osiele[1], Imosobomeh Lucky Ikhioya[3]*

[1] *Department of Physics, Delta State University, Abraka, Delta State, Nigeria*
[2] *Department of Physics, College of Education, Warri, Delta State, Nigeria*
[3] *Department of Physics, Federal University Lokoja, Nigeria*

Citation E.O Ojegu, A. Erhieyovwe, C.K. Ojoba, M.O. Osiele, I.L. Ikhioya, Improved Physical Properties of Zirconium Incorporation into the Iattice of Chromium Telluride Material. *J. Eng. Ind. Res.* **2026**, 7(2):76-88.

https://doi.org/10.48309/jeires.2026.550335.1315

Article info:
Submitted: 2025-09-30
Revised: 2025-10-22
Accepted: 2025-11-08
ID: JEIRES-2509-1315

Keywords:
Photovoltaic; Electrochemical deposition; Bandgap; Doping; Thin films.

ABSTRACT

The successful synthesis of undoped and doped CrTe was achieved through electrochemical deposition. The film exhibited a 2θ value of 46.51o and a hexagonal phase with orientations (111), (112), (121), and (200). The CrTe image exhibits a surface with compacted particles, indicating a favorable shaving surface. The absorption of photons is evident on the surface of the substrate with a well-packed grain size. The surface micrograph of the CrTe precursor was altererd by the addition of zirconium. The doped films exhibited a stone-like micro-grain in their surface morphology. As the dopant concentration increased, specific grains showed an enlargement and thickening of the stone-like nano-grains. The doped CrTe material successfully achieved a uniform deposition of nanoparticles across the entire solar substrate. There was a decrease in the material's thickness from 104.02 to 103.23 nm, accompanied by an increase in film resistivity from 5.49 to 6.03Ω.m. As a result, conductivity decreased from 1.82 to 1.65 S/m. The undoped exhibited an energy bandgap of 1.62 eV. The molar concentration of zirconium has an inverse relationship with the energy bandgap of doped CrTe, with the range decreasing from 1.68 eV at 0.1 mol, 1.42 eV 0.2 mol, and 1.41 eV 0.3 mol. Incorporating zirconium into the crystal lattice of chromium telluride (CrTe) introduces novel and distinct physical properties, primarily by modifying its optical and electrical characteristics. The key novelty is demonstrating a non-linear relationship between Zr concentration and surface morphology. The study identifies that 0.02 mol of Zr is the ideal amount for achieving superior dispersion and the finest grain structure. It also provides a clear mechanistic explanation for why a higher concentration (0.03 mol) fails, due to particle agglomeration.

Introduction

Achieving better performance, usability, and integration density at lower costs requires the use of semiconductor layers, insulators, and high-quality metals. The downsizing of integrated circuits has improved the quality of materials. Their optical and electrical qualities are exceptional. The intense doping of these semiconductors fundamentally

***Corresponding Author: Imosobomeh Lucky. Ikhioya** (imosobomeh.ikhioya@fulokoja.edu.ng)

alters their electronic band structure, leading to a suite of exceptional and highly tunable optical and electrical properties that deviate significantly from their intrinsic, undoped counterparts. This enhancement is not merely incremental; it enables entirely new functionalities by pushing the material toward a metallic state [1-4]. Semiconductor materials have been extensively studied due to their suitability for various devices such as LEDs, SETs, interference filters, photoconductors, IR detectors, and solar cells [5]. Chalcogenide materials have gained significant attention in scientific fields due to their exceptional qualities, including broad bandgap and excellent chemical, and thermal stability [6]. II-VI group compound semiconducting materials play a crucial role in various devices such as photovoltaic cells, LEDs, transistors, light sensors, and lasers [7-12]. Different researchers have examined the morphological, structural, optical, electrical, and dielectric properties of binary compounds, which are significant semiconducting chalcogenide materials [13-19]. These materials possess a wide bandgap and find applications in diverse semiconducting fields. By studying the morphological, structural, optical, electrical, and dielectric functions of chalcogenide materials, multiple researchers have discovered how doping can change their inherent characteristics [20,21]. Changing the characteristics of an intrinsic semiconductor involves introducing impurities. Doping has been employed in various endeavors to enhance the efficiency of semiconductors. Due to advancements in leakage current, remanent polarization, and fatigue durability, zirconium is considered as a highly promising dopant [22-25]. Zirconium can exist in two ionic states: acceptor and donor. Alterations in the bandgap and electrical properties occur due to zirconium doping.

A new 2D ferromagnet, chromium telluride (CrTe), was effectively synthesized by Wang *et al.* [26] using the CVD method. The magnetism of CrTe was investigated using the magneto-optical Kerr effect (MOKE) technique. Their study revealed that CrTe flakes display strong perpendicular anisotropy and hard magnetism. The magnetic properties remain strong as the thickness ranges from 45 nm to 11 nm, with the Curie temperature (TC) dropping from 205 K to 140 K. This study suggests a potential use for this ultrathin hard magnetic material in spintronic devices. Tube-in-tube chemical vapor deposition (CVD) growth technology was used by Chen *et al.* [27] to synthesize air-stable 2D Cr_5Te_8 ultrathin crystals with adjustable thickness. The synthesis of high-quality Cr_5Te_8 with precise composition relies on tube-in-tube CVD growth, which suppresses decomposition and promotes synthesis. By adjusting the growth temperature, the thickness of Cr5Te8 nanosheets changed from approximately 1.2 nm to tens of nanometers, leading to a transition in shape from triangle to hexagon. The Cr_5Te_8 nanosheet has been found to possess robust out-of-plane spin polarization and displays ferromagnetic behavior, as indicated by measurements using the magneto-optical Kerr effect. The Curie temperature of Cr_5Te_8 increases steadily from 100 to 160 K as its thickness goes from 10 to 30 nm, without any noticeable alterations in surface roughness or magnetic properties even after months of exposure to air. Their study progresses spintronics by presenting a dependable way to create top notch 2D ferromagnetic materials.

Chromium telluride (CrTe)'s special qualities make it suitable for many technological uses. CrTe's performance and function have been tested by researchers, using dopant element additions to its matrix. Zirconium (Zr) is now a well-regarded dopant. The physical properties of the material can be significantly enhanced by zirconium in the CrTe matrix [25]. The stability and performance of CrTe can be improved by utilizing zirconium's properties. Zr in the CrTe matrix helps create a solid solution by replacing chromium. Introducing substitutions can modify the crystal structure, lattice parameters, and electronic band structure of the material. The modifications can directly change how the CrTe-Zr composite behaves. With the addition of Zr to CrTe, the bandgap is altered, which enhances its use in optoelectronic tools like photodetectors, solar cells, and LEDs. Introducing Zr to CrTe may modify its magnetic behavior, possibly generating enhanced ferromagnetism or novel magnetic phases. Incorporating Zr into the CrTe matrix leads to better thermal stability and mechanical characteristics. Long-term reliability and durability are crucial for improved stability.

Adding zirconium to chromium telluride improves its physical properties, making it suitable for technology [27]. Zr doping allows scientists to improve cutting-edge functional materials.

Precise control over Zr/CrTe thin films is possible via ECD, which uses deposition parameters. The properties of the material change when Zr in CrTe is controlled [1]. The ECD technique enables uniform and homogeneous deposition of Zr/CrTe films on the substrate. Consistent and reproducible material properties are crucial for real-world applications. ECD is a low-temperature method, unlike other high-temperature techniques. The Zr/CrTe material's structure remains intact during low-temperature processing, avoiding degradation or phase changes. The ECD method is cheaper than other thin-film deposition methods because it uses simple, inexpensive tools [9-11]. Large-area deposition with ECD is easily scalable, which is greatly beneficial for industrial production. The adaptable ECD technique suits various substrates, such as metals, semiconductors, and insulators. This adaptability allows Zr/CrTe films to be used in multiple devices and technologies. Compared to PVD and CVD, ECD allows for better control of the composition, microstructure, and properties of the Zr/CrTe material. ECD is favored for Zr/CrTe films because it enables control over material performance.

The possible technological applications of CrTe and its compounds, such as thermoelectrics, catalysis, and energy storage, are already being explored by scientists. Zr/CrTe materials could be easily integrated into current tech frameworks using existing knowledge and infrastructure [24]. Exploring Zr's inclusion in CrTe reveals how dopants affect material traits. A more complete view of how doping affects complex materials aids in the intelligent design and optimization of advanced materials [26,27]. Zr/CrTe materials aims to improve chromium telluride's characteristics.

The physical properties of Zr-doped CrS films were thoroughly analyzed by Ugwu *et al.* [28], with a specific focus on the impact of precursor temperature during an electrochemical deposition for photovoltaic applications. Visible light spectra show declining absorbance from 300 to 600 nm, while ultraviolet spectra show an increase from 650 to 1,100 nm. The transparency of chromium sulfide films is improved by doping them with zirconium at precursor temperatures between 45 and 55 °C. CrS and Zr-doped CrS have energy bandgaps between 2.35 and 3.33 eV. The crystallite size of CrS and Zr-doped CrS increases when the precursor temperature rises. The material's grains show enhancements in quality and development. The crystal structure of CrS and Zr-doped CrS films is altered by precursor temperature. These studies show that the film's crystal structure, composition, and grain size are affected by changes in the precursor temperature.

This research investigates the effects of doping levels on zirconium-doped chromium telluride. The method is being applied innovatively to analyze the properties of the films, including their morphology, optics, electrical conductivity, and structure.

Preparation of FTO substrate

The FTO substrate was coated with undoped and doped CrTe. The area covered by the FTO-immersed region was approximately 2.5 cm^2. Before deposition, the FTO was cleaned for 15 minutes in ultrasonic baths containing ethanol, acetone, distilled water, and ammonia water. Drying of the FTO took place in an electric thermostatic oven at 65 °C for a specific duration. FTO is highly transparent in the visible spectrum due to its wide bandgap, which makes it perfect for solar cells and optoelectronic devices. The material's low electrical resistivity is due to a high concentration of free carriers from oxygen vacancies and fluorine doping, which improves its conductivity as a substrate. Compared to other conducting glasses, FTO's chemical stability enhances its durability and reliability under different experimental conditions.

Synthesis of the material

A solution with 0.1 M concentration, 10 mL in volume, was mixed with a 20/25 mL electrolyte solution of chromium (III) chloride, 10 mL of 0.1 mol of tellurium dioxide, and 5 mL of 0.1 to 0.4

mol of zirconium (IV) oxychloride octahydrate was used to conduct the ECD of undoped and doped CrTe. Figure 1 illustrates the ECD setup, which has a DC power supply connected to a three-electrode cell. In each experiment at room temperature, the deposition was held steady for 5 seconds at a voltage of 10 V and pH of 5.8. Under controlled parameters, the synthesized undoped and doped CrTe were subjected to testing. The 10 V potential deposition process occurred in a 50 mL beaker with solvents. Establishing the electrochemical bath hinged on the essential change in dopant molar concentrations from 0.1 to 0.4 mol. A total of 10 mL of chromium precursor and 5 mL of zirconium precursor was used to fill the bath system. The material's tension was released by heating the resulting samples to 220 °C for 35 minutes. The films' structural properties were analyzed using a Bruker D8-Advance X-ray diffractometer in continuous-scan with Cu-Kα radiation (λ= 1.5406 Å). MIRA3 TESCAN scanning electron microscopy was conducted to analyze the films' surface morphology. Using the 756S UV-Visible spectrophotometer, the the wavelength measurementss of the optical material were taken in a range from 300 to 1,100 nm. By subjecting the absorbance values to optical spectral analysis, the films' extra optical and solid-state features were deduced. Their electrical properties were investigated using the Jandel four-point probe method.

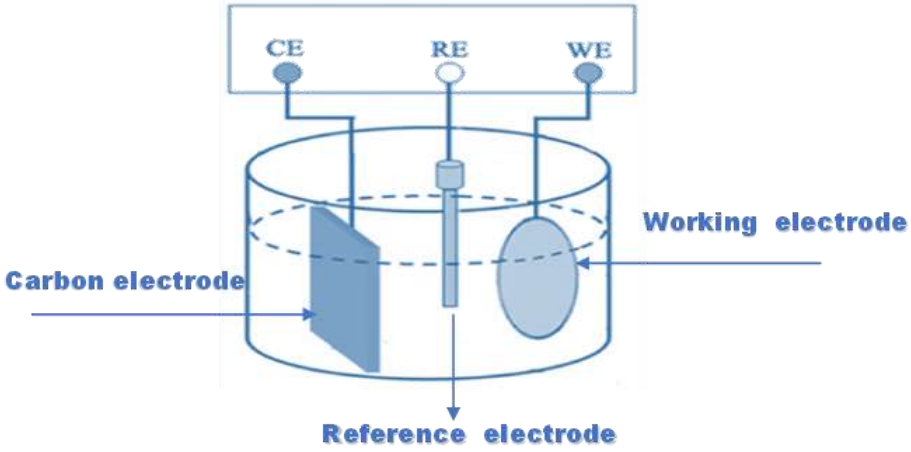

Figure 1: Schematic diagram of the ECD technique.

Optical analysis

Figure 2 (F1) provides a visual representation of the absorbance for undoped and doped CrTe material. The absorptivity of the material decreases as its wavelength increases. From the ultraviolet region to near-infrared, the film's absorbance decreases and reaches its highest point in the UV region. Decreases in the molarity of the films lead to a decrease in the doped films in the ultraviolet region, but an increase in the visible area occurs with a higher molar concentration of zirconium. The material that has been doped shows moderate absorption in both regions of the spectra, making it perfect for manufacturing solar plates used in industrial photovoltaic applications. In Figure 2 (F2), the transmittance spectra of undoped and doped CrTe at different levels of dopant concentration are displayed. The increase in transmittance of the films correlates with the wavelength of the incident light radiation. The film is most opaque to visible light and less opaque to near-infrared. As zirconium molarity increases, UV region film concentration increases while the visible region sees a small decrease. Due to its transmittance, the doped material is ideal for solar panels in each spectral region. Figure 2 (F3) shows the reflectance spectra of both undoped and doped CrTe, which were created using varying dopant molarity. Reflectance rises with increasing wavelength in the ultraviolet. The film's reflectance peaks in the visible spectrum, then

declines toward near-infrared. Increasing the molarity of the films leads to a decrease in the doped films in the UV area, and a slight increase in the visible area with higher molar concentrations of zirconium. The doped material displays moderate reflectance in both spectral regions, offering a practical choice for manufacturing photovoltaic solar plates

The energy bandgap was assessed by utilizing Equation (1) [5,11,13].

$$(\propto \mathrm{hv})^2 = \mathrm{A}(\mathrm{hv} - \mathrm{E_g}) \qquad (1)$$

Figure 2 (F4) shows a graph of $(\alpha hv)^2$ against hv for the synthesized film's energy bandgap at varied dopant concentrations. The straight portion of the graph was used to calculate the energy bandgap of the materials through extrapolation. An energy bandgap of 1.62 eV for the pristine CrTe was obtained. For Zr/CrTe, which was synthesized at a different molar concentrations of zirconium, the bandgap energy ranges from 1.68 eV at 0.1 mol, 1.42 eV 0.2 mol, and 1.41 eV 0.3 mol, indicating a decrease in energy bandgap as the molar concentration of zirconium increases.

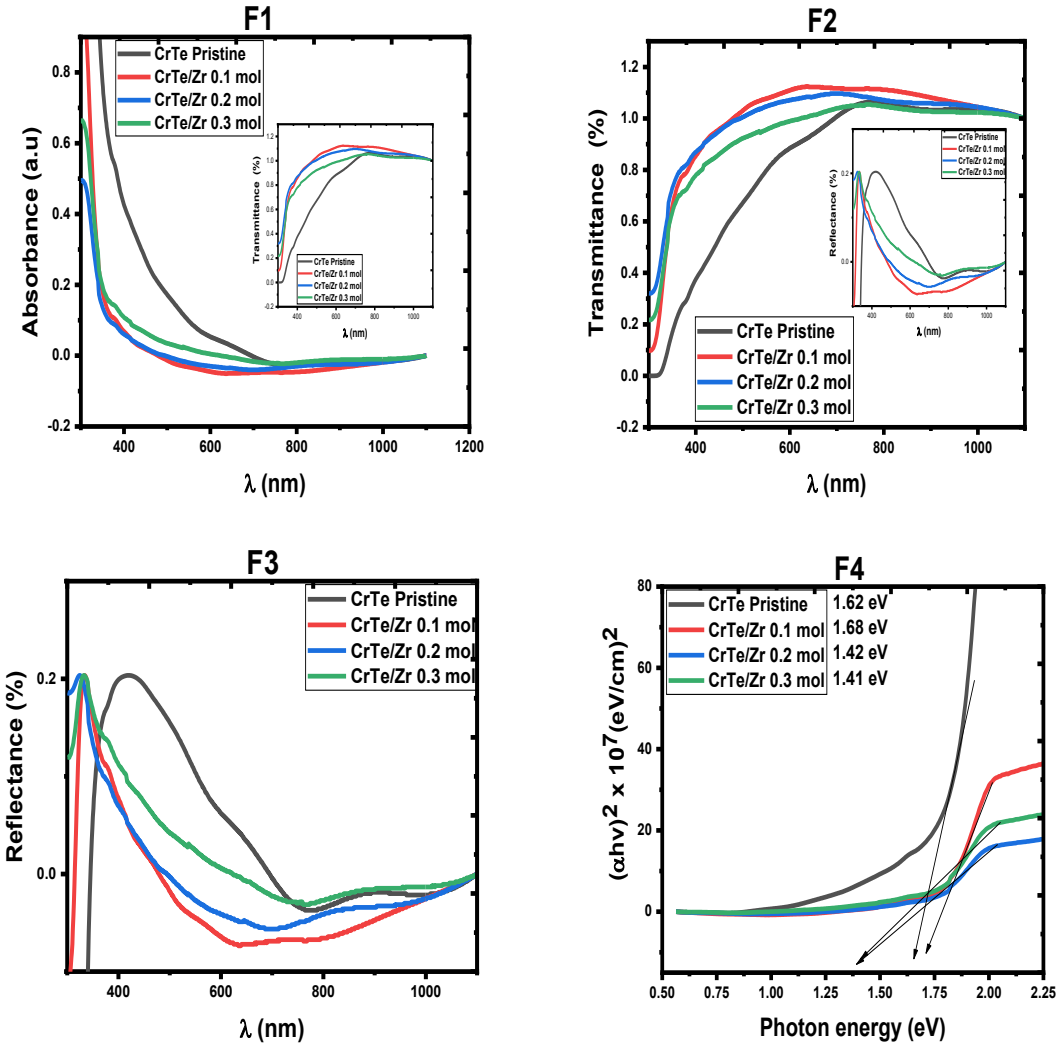

Figure 2: Absorbance (F1), transmittance (F2), reflectance (F3), and bandgap (F4).

$$n = \frac{1+\sqrt{R}}{1-\sqrt{R}} \quad (2)$$

$$\sigma opt. = \frac{\alpha nc}{4\pi} \quad (3)$$

$$K = \frac{\propto \lambda}{4\pi} \quad (4)$$

$$\varepsilon r = n^2 + k^2 \quad (5)$$

$$\varepsilon i = 2nk \quad (6)$$

The refractivity of the material was evaluated using Equation (2) [5-11,13], as depicted in Figure 3 (F5). Due to the increased molar concentration of the dopant, the material's refractivity experiences a sharp increase. In terms of the visible part of the spectrum, the pristine material possesses the highest refractivity. Increasing photon energy leads to a rise in the refractivity of the doped material. The plots illustrate how the molar concentration of the dopant influences the synthesized material. The refractive index of the films rises as the molar concentration of zirconium increases, benefiting both electronic industries and photovoltaic applications. The films' optical conductivity and extinction coefficient were determined using Equations (3 and 4) [5,11,13], and the results are shown in Figure 3 (F6 & F7). An increase in the molar concentration of zirconium leads to a sharp rise in the optical conductivity and extinction coefficient of the films. In the visible range, the pristine film's spectra show the greatest optical conductivity. In doped films, increased photon energy results in greater optical conductivity and extinction coefficient values. The synthesized films' response to zirconium molar concentration is shown in these plots. Zirconium's molar concentration directly boosts the films' optical conductivity/extinction, perfect for solar panels and lighting materials needing low extinction/high conductivity in electronics. Figure 4 (F8 & F9) illustrates the values of the real and imaginary dielectric constants of the films, obtained using Equations (5 and 6) [5,11,13]. The films experience a notable increase in dielectric constant as the concentration of zirconium increases. By examining the spectra, the real dielectric constant of the pristine film reached its maximum in the visible region, while the doped films showed an increase in the real dielectric constant as photon energy rises. The synthesized films' plot exhibits the substantial influence of zirconium molar concentration. Increasing the molar concentration of zirconium results in a higher real dielectric constant of the films, which is advantageous for photovoltaic applications in the electronic industry's solar panels and lighting systems. The imaginary dielectric constant undergoes a sharp growth due to the heightened photon energy displayed in Figure 4 (F9). The imaginary dielectric constant of the films is found to decrease as the molar concentration increases.

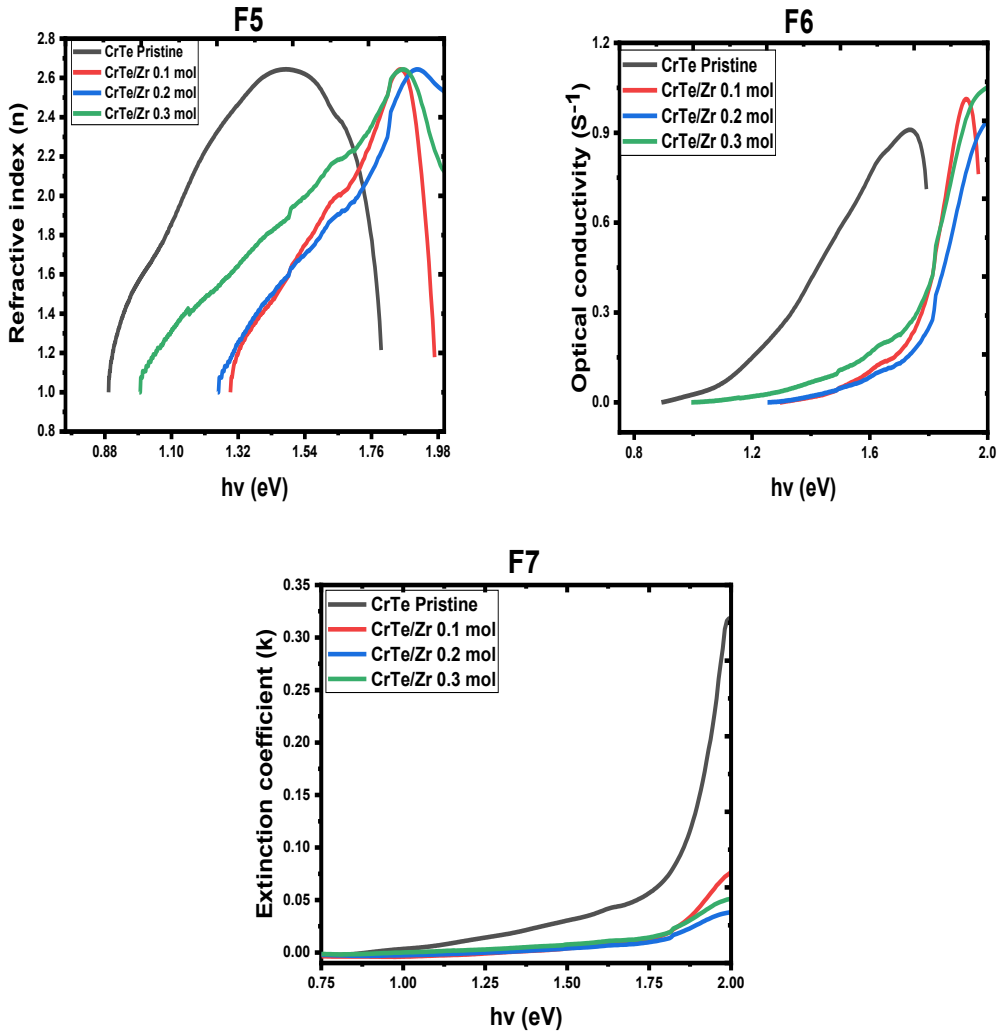

Figure 3: Refractive index (F5), optical conductivity (F6), and extinction coefficient (F7).

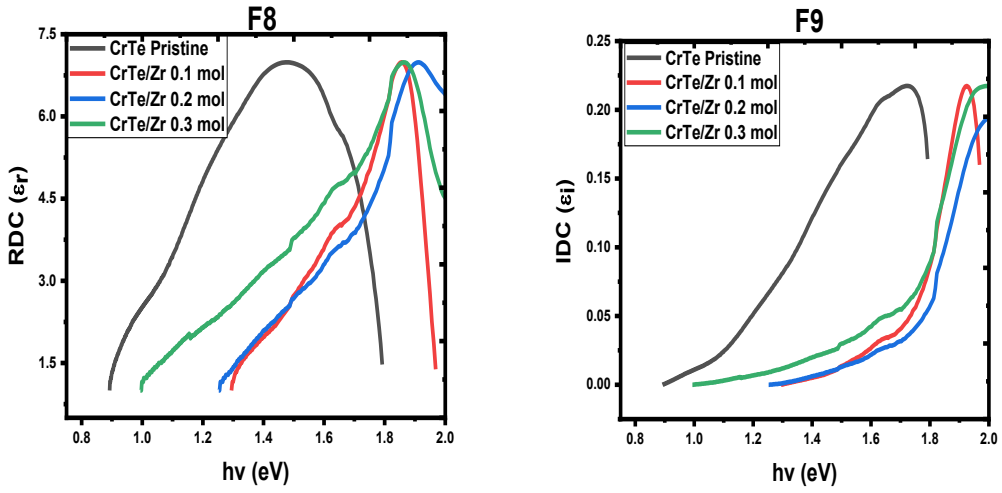

Figure 4: Real dialectric constant (F8), and imaginary dielectric constant (F9).

XRD analysis

Figure 5 illustrates the XRD patterns of undoped and doped CrTe with dopant molarities of 0.1 mol, 0.2 mol, and 0.3 mol. Polycrystalline materials comprise the composition of the material. A diffraction peak at (121) was observed in the film, with a corresponding 2θ value of 46.51°. The hexagonal phase exhibited a perfect diffraction peaks at (111), (112), (121), and (200), with 2θ angles of 21.57°, 32.79°, 46.51°, and 60.41°, respectively. Higher 2θ degree values show a decrease in peak intensity, which suggests the crystal lattice. The effectiveness of polycrystalline materials in photovoltaic and solar fabrication is due to their inherent nature. The higher peaks in the spectrum could be attributed to the increased surface area available for solar cells and photovoltaic systems, resulting from the film's thickness and higher dopant concentration. The crystallite or grain sizes, spectral parameters, and average crystallite size of the films are listed in Table 1. By applying Scherrer's equation, the crystallite size, lattice constants, inter-planar distance, and dislocation densities were evaluated and recorded in Table 1. The results were crucial in determining the best orientation at the (121) plane. By introducing dopants and adjusting crystallite sizes, the changes in lattice constants and dislocation densities were accounted for. A decrease in crystallite size leads to changes in lattice sites, causing an increase in both 2θ values and variable lattice constant values. Experiments have proven that the interplanar spacing varies across different orientation planes. Introducing the dopant induces distortions that lead to changes in the lattice structure, allowing the dopant to occupy the interstitial position. The reason for the broadening observed at higher 2θ values can be attributed to these aberrations. The broadening of the peak occurred at higher 2θangles as the crystallite size decreased [29]. To determine the structural properties in Table 1, such as the average crystallite size, D, the d-spacing, d, and the lattice constant, Scherrer's mathematical relation and Equations (7-9) [5,11,13] were employed.

$$D = {k\lambda}/{\beta\cos\theta} \quad (7)$$

$$d = {\lambda}/{2\sin\theta} \quad (8)$$

$$a = d\sqrt{h^2 + k^2 + l^2} \quad (9)$$

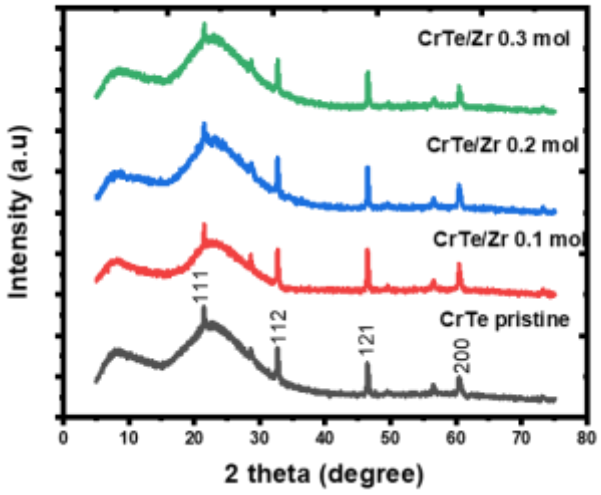

Figure 5: XRD pattern for CrTe and Zr/CrTe.

Table 1: Structural characteristics of undoped and doped CrTe material

Specimen	2θ (Degree)	(hkl)	d- spacing Å	Lattice constant (Å)	FWHM(β)	Crystallite size (nm)	Dislocation density	Strain
CrTe undoped	21.5721	111	4.1155	7.1284	0.1851	7.6226	4.6011	0.0191
CrTe/Zr 0.1mol	32.7917	112	2.7285	5.4571	0.2095	6.8963	5.5352	0.0812
CrTe/Zr 0.2mol	46.5161	121	1.9505	3.9010	0.1482	6.1974	2.0911	0.0795
CrTe/Zr 0.3mol	60.4119	200	1.5308	3.4231	0.2258	5.1043	3.6802	0.0902

Surface morphology of the material

The micrograph in Figure 6 shows the agglomeration of pinhole-free films and the compact grain size in undoped and doped CrTe. The undoped image displays a well-packed shaving surface with densely packed particles. Observations of photon absorption are made on the substrate surface , which has a well-packed grain size. The surface micrograph of the films revealed a noticeable change when zirconium was included as a dopant in the CrTe precursor. Observations of the doped films indicate a surface morphology resembling stone micrograins. Certain grains experienced an increase in size and thickness of the stone-like nanograin with the rise in dopant concentration. Using the doped CrTe material, nanostructures were evenly distributed across the entire solar substrate. By introducing 0.01 mol of Zr, the surface morphology is modified as it affects grain growth and enhances structural stability. With 0.02 mol of Zr, the surface morphology displays finer grains than the 0.01 mol variant, suggesting improved Zr dispersion. With 0.03 mol of Zr, the morphology demonstrates signs of agglomeration, causing the formation of larger grain clusters. Photovoltaic and optoelectronic devices benefit from the organized surface of the synthesized material. Figure 7 illustrates the elemental spectra of undoped and doped CrTe films. The spectrum reveals distinct peaks for chromium, tellurium, and the dopant zirconium. The elemental composition of the FTO substrate includes another element observed in the spectrum.

The resistivity and conductivity of undoped and doped CrTe at different dopant concentrations are shown in Table 2 and Figure 8 (F10 and F11). The thickness of the materials decreases from 104.02 to 103.23 nm, while the film resistivity increases from 3.21 x 10^{-3} to 6.03 x 10^{-3}Ω.m. As a result, conductivity drops from 3.11 x 10^{6} to 1.65 x 10^{6} S/m. The materials were deposited using dopant molarities of 0.1 mol, 0.2 mol, and 0.3 mol. Due to their high resistivity and low conductivity, the produced films are suitable for photovoltaic and solar applications. As the film thickness decreases, Figure 8 (F10) illustrates the manifestation of high resistivity and low conductivity. Figure 8 (F11) showcases a nonlinear graph demonstrating the relationship between zirconium dopant and resistivity/conductivity fluctuations.

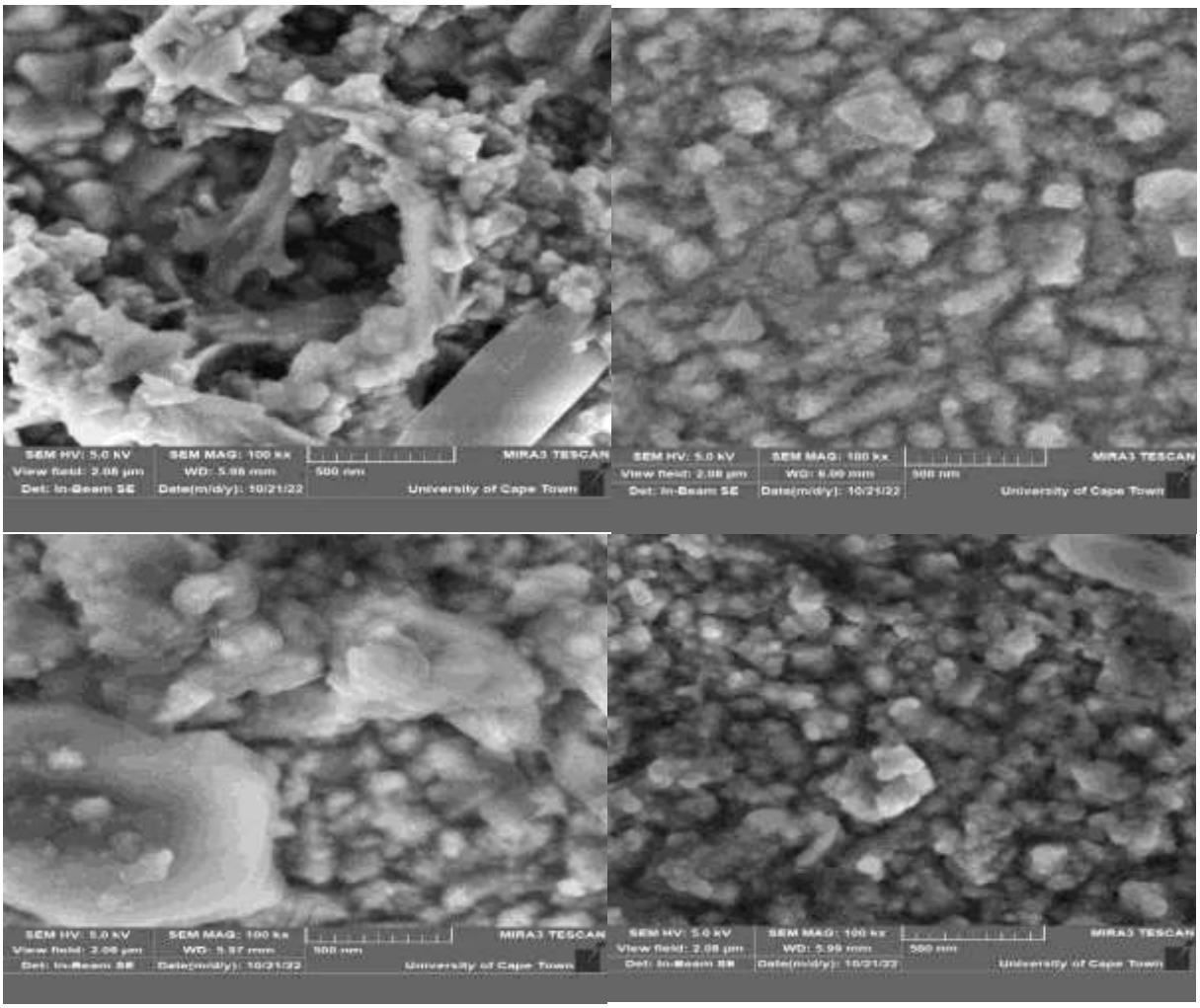

Figure 6: Surface image of undoped and doped CrTe.

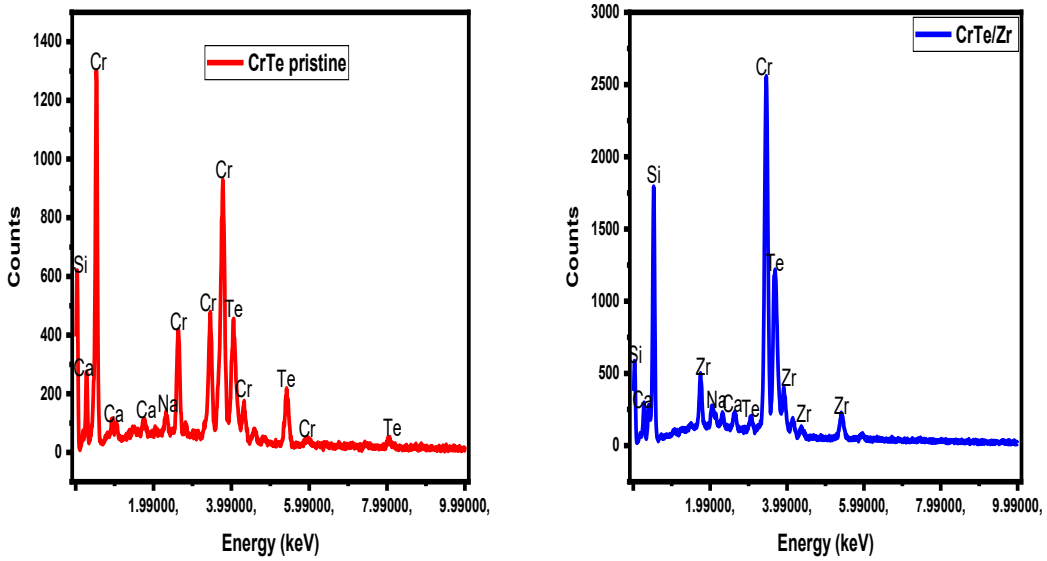

Figure 7: EDX of undoped and doped CrTe.

Electrical study of the material.

Using Equations (10-12) [5,11,13], the resistivity and conductivity of the samples were determined.

$$R_s = R\left({}^{V}/_{I}\right) \quad (10)$$

Where, $K = {}^{\pi}/_{ln2}$

$$\rho = t \times R_s \quad (11)$$

$$\sigma = {}^{1}/_{\rho} \quad (12)$$

Table 2: Electrical properties of undoped and doped CrTe

Specimen	T (nm)	ρ (Ω.m) × 10^{-3}	σ (S/m) × 10^{6}
CrTe undoped	104.02	5.49	1.82
CrTe/Zr 0.1 mol	103.13	3.21	3.11
CrTe/Zr 0.2 mol	103.18	4.02	2.48
CrTe/Zr 0.3 mol	103.23	6.03	1.65

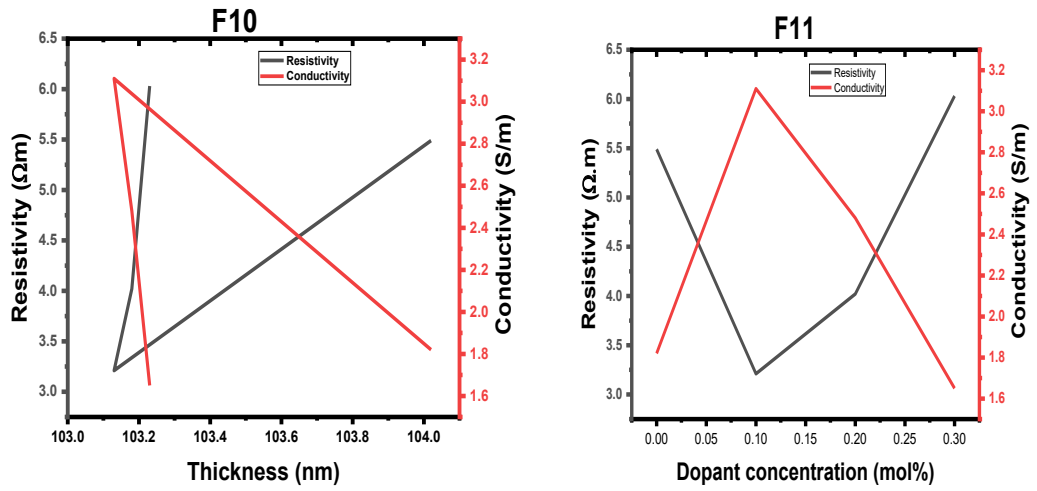

Figure 8: Resistivity and conductivity vs. film thickness F10) and (resistivity and conductivity versus dopant concentration F11).

Conclusion

The synthesis of undoped and zirconium-doped CrTe thin films was achieved using electrochemical deposition (ECD). The hexagonal phase confirmed in films through structural analysis, and doping affects the material's properties. Zirconium's addition allows firm control over the film's surface, electrical nature, and optical bandgap. By adjusting the molar concentration of the Zr dopant, the bandgap was precisely tuned between 1.86 eV and 1.41 eV. The observed changes in film resistivity and conductivity, along with this tunability, prove the effectiveness of doping in CrTe property engineering. The results of this study are very useful in research and industry, especially in

optoelectronics and renewable energy. Zr/CrTe's tunable bandgap, dropping to 1.41 eV, suggests it could be a great absorber layer in thin-film solar cells. This value nearly matches the optimal bandgap (1.34 eV) for maximum theoretical solar conversion efficiency, implying that Zr/CrTe-based devices might perform well. ECD's commercial potential is further boosted by a cheap, scalable synthesis method. This research details a clear path to making bespoke semiconductor materials. This can lead to new electronic components for the industry. Controlling grain size and structural stability is vital for device reliability. The surface morphology is highly dependent on the Zr concentration. The introduction of 0.01 mol of Zr modifies the surface by influencing grain growth and improving structural stability. A higher concentration of 0.02 mol of Zr further refines the grain structure, which is attributed to a more homogeneous dispersion of Zr within the matrix. Conversely, an excessive amount of Zr (0.03 mol) induces particle agglomeration, resulting in the formation of larger, less uniform grain clusters.

Conflicts of Interest

No conflicts of interest were reported by the authors in this study.

Funding

The authors conducted this research without financial support.

Ethics Approval

The research and analysis are accurately portrayed in the publication.

Data Availability Statement

Upon request, the corresponding author can furnish the data that backs up the study's conclusions.

ORCID

Ernest Ogheneruona Ojegu
https://orcid.org/0009-0002-2947-1896
Akpata Erhieyovwe
https://orcid.org/0009-0008-2111-6017
Clever Kate Ojoba
https://orcid.org/0009-0004-5055-931X
Mike Onyekachukwu Osiele
https://orcid.org/0009-0006-5019-6322
Imosobomeh Lucky Ikhioya
https://orcid.org/0000-0002-5959-4427

Reference

[1] Samuel, S.O., James, F.E., JT, Z., EP, O., Ekpekpo, A., Ikhioya, I.L. Effect of dopant on the energy bandgap on strontium sulphide doped silver for optoelectronic application. *Materials Research Innovations*, **2024**, 28(1), 8-18.
[2] Ikhioya, I.L., Ugwuoke, C.O., Ochai-Ejeh, F.U. Optimisation of temperature regulator on spray pyrolysis cobalt selenide doped erbium (CoSe: Er) semiconductor material for photovoltaic application. *Materials Research Innovations*, **2024**, 28(1), 32-39.
[3] Sreenivasan, M., Bi, J., Teo, K., Liew, T. Systematic investigation of structural and magnetic properties in molecular beam epitaxial growth of metastable zinc-blende CrTe toward half-metallicity. *Journal of applied Physics*, **2008**, 103(4), 43908.
[4] Yang, X., Zhou, X., Feng, W., Yao, Y. Tunable magneto-optical effect, anomalous Hall effect, and anomalous Nernst effect in the two-dimensional room-temperature ferromagnet 1*T*-$CrTe_2$. *Physical Review B*, 2021, 103(2), 024436.
[5] Akpu, N.I., Asiegbu, A., Nnanna, L., Ikhioya, I., Mgbeojedo, T. Investigation on the influence of varying substrate temperature on the physical features of yttrium doped cadmium selenide thin films materials. *SSRG International Journal of Applied Physics*, **2021**, 8(2), 37-46.
[6] Ikhioya, I., Okeoghene, I., AC, B., Josephine, O., Yahaya, A. Effect of Precursor pHon Cadmium Doped Manganese Sulphide (CdMnS) Thin Films for Photovoltaic Application. *International Journal of Material Science and Engineering*, **2020**, 6(2), 1-8.
[7] Ikhioya, I.L., Okoli, D., Ekpunobi, A.J. Effect of temperature on SnZnSe semiconductor thin films for photovoltaic application. *SSRG International Journal of Applied Physics*, **2019**, 6(2), 55-67.
[8] Ogbonnaya, O.C. The Influence of precursor temperature on the properties of Erbium-Doped Zirconium Telluride thin film material via electrochemical deposition. *International Journal of Applied Physics*, **2020**, 102.
[9] Bouriche, A., Benouis, C., Benhaliliba, M., Dris, K. AI Bridges theory and practice: 18% efficient SIS solar cells via defect-tuned ZnO/TiO_2/p-Si structure.

Journal of Engineering in Industrial Research , **2025**, 6(4), 282-297.
[10] Ojegu, E.O., Ikhioya, I.L. Investigating the Impact of Temperature on MgSe Structural, Optical and Electrical Features to Optimize its Use in Optoelectronics. *Journal of Engineering in Industrial Research*, **2024**, 5(1), 16-26.
[11] Ugwu, L.U., Ikhioya, I.L., Ekpunobi, A.J. Influence of Precursor Temperature on the Bandgap Engineering of Zr-Doped CrS for Photovoltaic Application. *Journal of Engineering in Industrial Research*, **2024**, 5, (1) 52 64.
[12] Lucky, I.I., Ugbo, F., Ijabor, B.O. Growth and characterization of manganese sulphide (MnS) thin films. *International Journal for Research in Applied and Natural Sciences*, **2018**, 4(1), 1-9.
[13] Ikhioya, I.L., Whyte, G.M., Nkele, A.C. Temperature-modulated nanostructures of ytterbium-doped Cobalt Selenide (Yb-CoSe) for photovoltaic applications. *Journal of the Indian Chemical Society*, **2023**, 100(1), 100848.
[14] Udofia, K.I., Ikhioya, I.L., Agobi, A.U., Okoli, D.N., Ekpunobi, A.J. Effects of zirconium on electrochemically synthesized tin selenide materials on fluorine doped tin oxide substrate for photovoltaic application. *Journal of the Indian Chemical Society*, **2022**, 99(10), 100737.
[15] Yang, H., Wu, A., Yi, H., Cao, W., Yao, J., Yang, G., Zou, Y.C. Atomic scale insights into the epitaxial growth mechanism of 2D Cr_3 Te_4 on mica. *Nanoscale Advances*, **2023**, 5(3), 693-700.
[16] Zhang, S., Wu, H., Yang, L., Zhang, G., Xie, Y., Zhang, L., Chang, H. Two-dimensional magnetic atomic crystals. *Materials Horizons*, **2022**, 9(2), 559-576.
[17] Jiang, X., Chen, F., Zhao, S., Su, W. Recent progress in the CVD growth of 2D vertical heterostructures based on transition-metal dichalcogenides. *CrystEngComm*, **2021**, 23(47), 8239-8254.
[18] Chen, C., Chen, X., Wu, C., Wang, X., Ping, Y., Wei, X., Zhou, J. Air-stable 2D Cr_5Te_8 nanosheets with thickness-tunable ferromagnetism. *Advanced Materials*, **2022**, 34(2), 2107512.
[19] Sun, S., Liang, J., Liu, R., Shen, W., Wu, H., Tian, M., Lin, W. Anisotropic magnetoresistance in room temperature ferromagnetic single crystal CrTe flake. *Journal of Alloys and Compounds*, 2022, 890, 161818.
[20] Wang, Y., Kajihara, S., Matsuoka, H., Saika, B.K., Yamagami, K., Takeda, Y., Nakano, M. Layer-number-independent two-dimensional ferromagnetism in Cr_3Te_4. *Nano Letters*, **2022**, 22(24), 9964-9971.
[21] Yang, Y., Jia, L., Wang, D., Zhou, J. Advanced strategies in synthesis of two-dimensional materials with different compositions and phases. *Small Methods*, **2023**, 7(4), 2201585.
[22] Luo, F.S., Ying, J.S., Zhang, Y., Li, S.S., Tang, F., Chen, T.W., Zheng, R.K. The effects of substrate temperature on the magnetic and magnetotransport properties of $Cr_{1-x}Te$ epitaxial films. *Journal of Magnetism and Magnetic Materials*, **2022**, 550, 169084.
[23] Guo, Y., Kang, L., Yu, S., Yang, J., Qi, X., Zhang, Z., Liu, Z. CVD growth of large-scale and highly crystalline 2D chromium telluride nanoflakes. *ChemNanoMat*, **2021**, 7(3), 323-327.
[24] Kraschinski, S., Herzog, S., Bensch, W. Low temperature synthesis of chromium tellurides using superlattice reactants: crystallisation of layered $CrTe_3$ at 100° C and the decomposition into Cr_2Te_3. *Solid State Sciences*, **2002**, 4(10), 1237-1243.
[25] Yang, J., Zhu, C., Deng, Y., Tang, B., Liu, Z. Magnetism of two-dimensional chromium tellurides. *Iscience*, **2023**, 26(5).
[26] Wang, M., Kang, L., Su, J., Zhang, L., Dai, H., Cheng, H., Han, J. Two-dimensional ferromagnetism in CrTe flakes down to atomically thin layers. *Nanoscale*, **2020**, 12(31), 16427-16432.
[27] Chen, C., Chen, X., Wu, C., Wang, X., Ping, Y., Wei, X., Zhou, J. Air-stable 2D Cr_5Te_8 nanosheets with thickness-tunable ferromagnetism. *Advanced Materials*, **2022**, 34(2), 2107512.
[28] Ugwu, L.U., Ikhioya, I.L., Ekpunobi, A.J. Influence of Precursor Temperature on the Bandgap Engineering of Zr-Doped CrS for Photovoltaic Application. *Journal of Engineering in Industrial Research*, **2024**, 5(1), 52-64.
[29] Arulanantham, A., Gunavathy, K., Rangasami, C., Thomas, R., Mohanraj, P., AlFaify, S., Shkir, M. Comprehensive investigation on ruthenium doped Sn_2S_3 thin films for photo sensing applications. *Physica B: Condensed Matter*, **2024**, 693, 416380.